IEEE Access
Multidisciplinary | Rapid Review | Open Access Journal

Received October 5, 2021, accepted October 27, 2021, date of publication November 8, 2021, date of current version November 12, 2021.

Digital Object Identifier 10.1109/ACCESS.2021.3125856

Drain Induced Barrier Widening and Reverse Short Channel Effects in Tunneling FETs: Investigation and Analysis

MAMIDALA KARTHIK RAM[1], NEHA TIWARI[1], DAWIT BURUSIE ABDI[2], AND SNEH SAURABH[3], (Senior Member, IEEE)

[1]Department of Electronics and Communication Engineering, NIIT University, Neemrana, Rajasthan 301705, India
[2]Technology Solutions and Enablement, IMEC, 3001 Leuven, Belgium
[3]Department of Electronics and Communication Engineering, IIIT Delhi, New Delhi 110020, India

Corresponding author: Mamidala Karthik Ram (karthikram37nc@gmail.com)

ABSTRACT In this paper, using calibrated TCAD simulations, we demonstrate how the performance of a Tunneling FET (TFET) can be improved by using a new phenomenon called drain induced barrier widening (DIBW) at the source-channel junction. Our results indicate that TFETs in which DIBW dominates exhibit a steep subthreshold swing (≈35 mV/dec) and a low OFF-state current (≈10^{-16}A/μm) without affecting the ON-state current. We also show that TFETs exhibit a reverse short channel effect due to an increase in the tunneling width at the source-channel junction.

INDEX TERMS Drain induced barrier widening (DIBW), gate-on-drain overlap, OFF-state current, reverse short channel effects, subthreshold swing, TCAD simulation, tunnel field effect transistor (TFET).

I. INTRODUCTION

With advantages such as a sub-60 mV/dec subthreshold swing (SS) at room temperature and a lower OFF-state leakage current, the tunnel field effect transistor (TFET) presents itself as a promising low power alternative to the conventional MOSFETs [1]–[6].

To enhance the performance of TFETs, different techniques have been attempted in the past such as bandgap engineering using a graded Si/Ge heterojunction TFET [7] and using dual spacer dielectrics [8]. Similarly, using a very lightly doped drain material ($N_D \approx 1 \times 10^{17}$ cm^{-3}) with low density of states (e.g. InGaAs), it has been shown that a reduction in OFF-state current and subthreshold swing can be obtained [9]. In such a structure, to reduce the drain series resistance, the length of the lightly doped drain should be limited to approximately 10 nm by backing it up with an n^+-contact [9]. It has been shown recently that by using a non-uniform body thickness in a TFET, the ON/OFF current ratio of TFETs can be improved. Realizing such a structure requires precise control of device dimensions, particularly the channel thickness [10]. TFETs are the potential candidates to surmount the performance challenges in transistors. Therefore, there is a great need to study the performance of TFETs using viable approaches required for future low power circuit applications.

In this paper, using calibrated two-dimensional simulations, we demonstrate that TFETs with low OFF-state leakage current and sub-60 mV/dec subthreshold swing can be realized without affecting the ON-state current using a new phenomenon called drain induced barrier widening (DIBW) at the source-channel junction. We show that the presence of DIBW leads to reverse short channel effects in TFETs as the channel length is reduced. Our results may pave the way, for realizing steep subthreshold TFETs with low OFF-state leakage current required in future low power integrated circuits. We discuss the device structure and the simulation parameter details in Section II and then present the simulation results in Section III. Finally, the conclusions are summarized in Section IV.

II. DEVICE STRUCTURE AND SIMULATION PARAMETERS

Fig. 1 shows the cross-sectional schematic views for (a) the TFET with no gate-on-drain overlap (conventional TFET), (b) the single material gate (SMG) TFET using gate-on-drain overlap with uniform thickness for the gate oxide and the

The associate editor coordinating the review of this manuscript and approving it for publication was Jesus Felez.

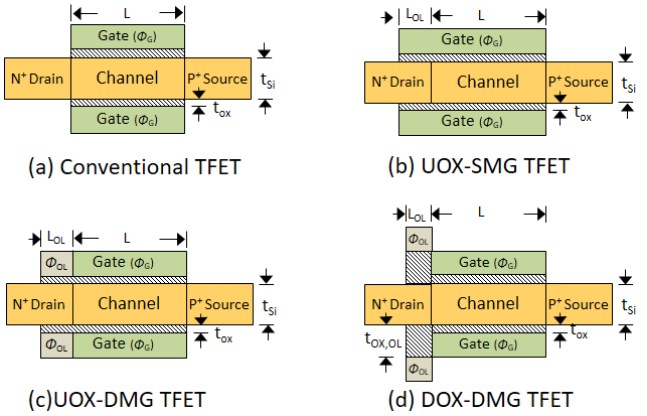

FIGURE 1. Cross-sectional views of (a) Conventional TFET, (b) UOX-SMG TFET, (c) UOX-DMG TFET and (d) DOX-DMG TFET.

oxide under the gate-on-drain overlap (UOX-SMG), (c) the dual material gate (DMG) TFET using gate-on-drain overlap with uniform thickness for the gate oxide and the oxide under the gate-on-drain overlap (UOX-DMG), and (d) the dual material gate TFET using gate-on-drain overlap with differential thickness for the gate oxide and the oxide under the gate-on-drain overlap (DOX-DMG).

The device parameters used in our simulations are shown in Table 1. We have used three different drain doping concentrations ($N_D = 1 \times 10^{18}$ cm^{-3}, 5×10^{18} cm^{-3} and 1×10^{19} cm^{-3}). For each of these drain doping concentrations, the gate work function (Φ_G) and the gate-on-drain overlap work function (Φ_{OL}) and the equivalent oxide thickness (EOT) under the gate-on-drain overlap ($t_{OX,OL}$), given in Table 1, are optimised for steeper subthreshold swing (SS) and low OFF-state current in DOX-DMG and UOX-DMG TFETs for L = 10 nm. The same gate work functions (Φ_G and Φ_{OL}) are then used in the other three structures. The length of the gate-on-drain overlap (L_{OL}) is chosen to be 30 nm in our study for the structures shown in Fig. 1 as this length has been shown to be the optimum gate-on-drain overlap length for reducing the ambipolar current in TFETs [11]. It has also been shown in [11], [12] that the AC performance of the device will not be impacted adversely by the gate-drain capacitance (C_{gd}) due to the gate-on-drain overlap. The gate-on-drain overlap and the step gate oxide required in this study can be realized using the fabrication techniques reported in [13]–[21].

III. SIMULATION APPROACH

All the simulations were done in Silvaco Atlas [22]. As described in [23], [24] our simulation set up was calibrated to the results in [4]. To take into account the lateral tunneling that takes place at the source-channel junction, we used a nonlocal band to band tunneling (BTBT) model. Due to the high doping concentration in the source and drain regions, the bandgap narrowing model is enabled. We used a concentration dependent model to include the mobility effects in our simulations. The Shockley-Read-Hall (SRH) recombination model and the Fermi Dirac statistics were also used. All the

TABLE 1. Device parameters used in simulations.

Parameters		No overlap	UOX-SMG	UOX-DMG	DOX-DMG
Channel Length, L (nm)		10 - 50	10 - 50	10 - 50	10 - 50
Silicon Body Thickness, t_{Si} (nm)		10	10	10	10
Gate Equivalent Oxide Thickness (EOT), t_{OX} (nm)		1.0	1.0	1.0	1.0
Channel Doping, N_A (cm^{-3})		1×10^{17}	1×10^{17}	1×10^{17}	1×10^{17}
Source Doping, N_A (cm^{-3})		1×10^{20}	1×10^{20}	1×10^{20}	1×10^{20}
Drain Doping, N_D (cm^{-3}) = 1×10^{18}	Φ_G (eV)	4.2	4.2	4.2	4.2
	Φ_{OL} (eV)	-	4.2	4.6	5.0
	$t_{OX,OL}$ (nm)	-	1.0	1.0	10
Drain Doping, N_D (cm^{-3}) = 5×10^{18}	Φ_G (eV)	4.3	4.3	4.3	4.3
	Φ_{OL} (eV)	-	4.3	5.3	5.3
	$t_{OX,OL}$ (nm)	-	1.0	1.0	5.0
Drain Doping, N_D (cm^{-3}) = 1×10^{19}	Φ_G (eV)	4.5	4.5	4.5	4.5
	Φ_{OL} (eV)	-	4.5	5.1	5.1
	$t_{OX,OL}$ (nm)	-	1.0	1.0	3.0

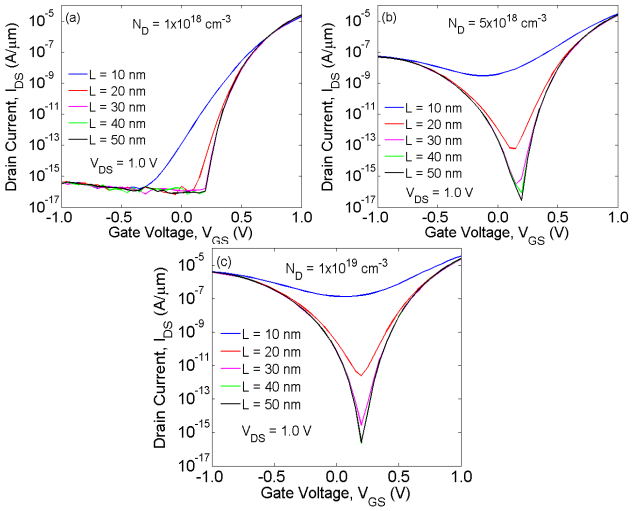

FIGURE 2. Transfer characteristics of a conventional TFET with work function $\Phi_G = 4.5$ eV, and L scaled from 50 nm to 10 nm for different drain doping concentrations: (a) $N_D = 1 \times 10^{18}$ cm^{-3}, (b) $N_D = 5 \times 10^{18}$ cm^{-3} and (c) $N_D = 1 \times 10^{19}$ cm^{-3}.

doping profiles are assumed to be abrupt in these simulations as previously done in [23], [24]. Quantum mechanical effects are not considered for $t_{si} \geq 7$ nm [5], [25]. Therefore, we have not included quantum mechanical effects in these simulations as we have limited t_{si} to 10 nm as previously done in [23], [24].

IV. RESULTS AND DISCUSSION

The transfer characteristics of a conventional TFET for different channel lengths and drain doping concentrations can be seen in Fig. 2. From Fig. 2 (a), we observe that even at the conventional drain doping concentration $N_D = 1 \times 10^{18}$ cm^{-3}, the transfer characteristics become non-ideal at a channel length of 10 nm and the TFET becomes unusable due to its poor subthrehsold swing and increased OFF-state current at $V_{GS} = 0.0$ V. This is in agreement with the previously reported results [7], [9], and makes the device unsuitable

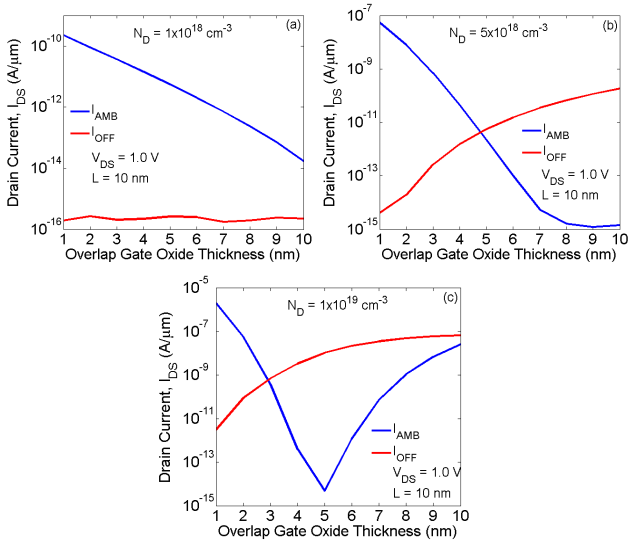

FIGURE 3. For a TFET with a gate-on-drain overlap ($\Phi_G = \Phi_{OL} = 4.5$ eV), comparison of the ambipolar current (I_{AMB}) and OFF-state current (I_{OFF}) versus the oxide thickness under the gate-on-drain overlap ($t_{OX,OL}$) for the doping concentrations: (a) $N_D = 1 \times 10^{18}$ cm^{-3}, (b) $N_D = 5 \times 10^{18}$ cm^{-3} and (c) $N_D = 1 \times 10^{19}$ cm^{-3}.

for future applications in low power integrated circuits. The performance deteriorates further with the additional disadvantage of ambipolar current for higher drain doping concentrations e.g. $N_D = 5 \times 10^{18}$ cm^{-3} and $N_D = 1 \times 10^{19}$ cm^{-3} as shown in Figs. 2 (b) and (c), respectively.

To obviate the problem of poor subthreshold swing and large OFF-state current associated with short channel TFETs, we have studied three different TFET structures with gate-on-drain overlap as shown in Fig. 1. For UOX-SMG and UOX- DMG TFET structures, we have used identical thickness for the gate oxide ($t_{OX,}$) and the oxide under the gate-on-drain overlap ($t_{OX,OL}$). For DOX-DMG TFET, the oxide thickness under the gate-on-drain overlap is higher than the gate oxide thickness. In the case of UOX-DMG TFET and DOX-DMG TFET, the work function of the gate-on-drain overlap (Φ_{OL}) is higher than the gate work function (Φ_G).

The oxide thickness under the gate-on-drain overlap in the DOX-DMG TFET needs to be optimized with the goal of finding a balance between the lowest OFF-state current as well as ambipolar current. Fig. 3 shows the ambipolar current (I_{AMB}) at $V_{GS} = -1.0$ V and the OFF-state current (I_{OFF}) at $V_{GS} = 0.0$ V versus the oxide thickness under the gate-on-drain overlap ($t_{OX,OL}$) for three different drain doping concentrations. In Fig. 3 (a), we observe that the ambipolar current continuously decreases while the OFF-state current remains nearly constant with increasing $t_{OX,OL}$. Therefore, we have chosen $t_{OX,OL} = 10$ nm for DOX-DMG TFET for $N_D = 1 \times 10^{18}$ cm^{-3}. In Fig. 3 (b), we observe that the ambipolar current decreases while the OFF-state current increases with increasing $t_{OX,OL}$. We note that, at $t_{OX,OL} \approx 5$ nm, the ambipolar current and OFF-state current are at an optimum value for $N_D = 5 \times 10^{18}$ cm^{-3}. In Fig. 3 (c), we observe that the ambipolar current initially decreases up to $t_{OX,OL} = 5$ nm and increases for higher $t_{OX,OL}$, while the OFF-state current increases continuously with increasing $t_{OX,OL}$. We note that, at $t_{OX,OL} \approx 3$ nm, the ambipolar current and OFF-state current are at an optimum value for $N_D = 1 \times 10^{19}$ cm^{-3}. Therefore, to examine the short channel behavior of DOX-DMG TFET, we have chosen $t_{OX,OL}$ to be 10 nm, 5 nm and 3 nm for $N_D = 1 \times 10^{18}$ cm^{-3}, 5×10^{18} cm^{-3} and 1×10^{19} cm^{-3}, respectively.

In the following sections, we analyze the impact of the gate-on-drain overlap by comparing the short channel behavior of all the four TFETs shown in Fig. 1 by calculating the average SS, point SS and I_{ON}/I_{OFF} ratio from the transfer characteristics.

The average SS for all the TFET structures in this work has been calculated using the following expression [5]:

$$Average\ SS = \frac{V_t - V_{Off}}{logI_{Vt} - logI_{Off}} \tag{1}$$

where the threshold voltage (V_t) is the applied gate voltage when the drain current reaches a magnitude of 1×10^{-7} A/μm, V_{off} is the gate voltage at which the lowest magnitude of the drain current is observed when the gate voltage $V_{GS} \geq 0.0$ V, I_{Vt} is the drain current at V_t and I_{Off} is the drain current at V_{Off}.

The point subthreshold swing is calculated as the reciprocal of the maximum slope of the transfer characteristics as given below [1]:

$$Point\ SS = \frac{dV_{GS}}{d\log(I_{DS})} \tag{2}$$

where I_{DS} is the drain current and V_{GS} is the gate voltage where the slope of the transfer characteristics is maximum.

In the following sections, we examine how the gate-on-drain overlap can be effectively used to realize steep subthreshold performance and low OFF-state current.

A. IMPACT OF THE GATE-ON-DRAIN OVERLAP ON TFETs FOR $N_D = 1 \times 10^{18}$ cm^{-3}

Fig. 4 shows the transfer characteristics, average SS and point SS of the four different TFET structures for L = 50 nm and 10 nm. In Figs. 4 (a) and (b), either for L = 50 nm or 10 nm, we observe that the conventional TFET exhibits no ambipolar current. It may be noted that when L is reduced from 50 nm to 10 nm, due to short channel effects, the conventional TFET exhibits an extremely poor average SS and point SS as shown in Figs. 4 (c) and (d), respectively. However, in the case of UOX-DMG and DOX-DMG TFETs with L = 10 nm, the gate-on-drain overlap leads to an average SS and point SS well below 60 mV/dec as compared to UOX-DMG and DOX-DMG TFETs with L = 50 nm. Therefore, the UOX-DMG and DOX-DMG TFETs with a lightly doped drain can indeed lead to TFETs with an OFF-state current $\approx 10^{-16}$ A/μm, an average SS well below 60 mV/dec, and I_{ON}/I_{OFF} ratio $> 10^{11}$ as shown in Fig. 5.

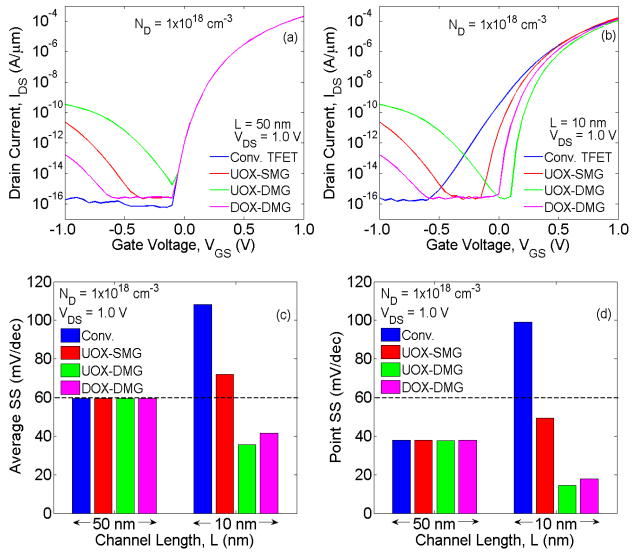

FIGURE 4. (a) Transfer characteristics for L = 50 nm, (b) transfer characteristics for L = 10 nm, (c) average SS and (d) point SS of the four different TFET structures with $N_D = 1 \times 10^{18}$ cm^{-3}.

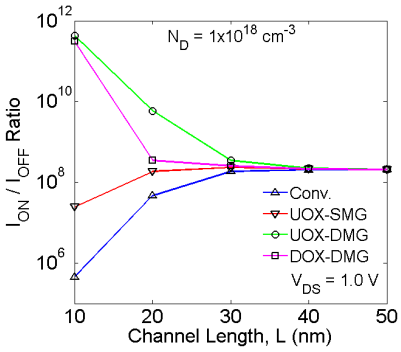

FIGURE 5. I_{ON}/I_{OFF} ratio versus channel length of the four different TFET structures where $I_{ON} = I_{DS}$ at $V_{GS} = 1.0$ V and $I_{OFF} = I_{DS}$ at $V_{GS} = 0.0$ V.

B. IMPACT OF THE GATE-ON-DRAIN OVERLAP ON TFETs FOR $N_D = 5 \times 10^{18}$ cm^{-3}

In Figs. 6 (a) and (b), either for L = 50 nm or 10 nm, we observe that all the four TFETs exhibit the presence of ambipolar current due to the higher drain doping concentration. When L is reduced from 50 nm to 10 nm, both the conventional TFET and UOX-SMG TFET show degraded average SS and point SS as shown in Figs. 6 (c) and (d), respectively.

As compared to the conventional TFET, we observe that the UOX-DMG TFET becomes unusable due to its large OFF-state current as shown in Figs. 6 (a) and (b). However, the DOX-DMG TFET exhibits improved performance with a low OFF-state current $\approx 10^{-14}$ A/μm, an average SS below 60 mV/dec and an I_{ON}/I_{OFF} ratio $\approx 10^{10}$ as shown in Fig. 7 when L is reduced from 50 nm to 10 nm. It is clear that the DOX-DMG TFET with a higher drain doping concentration ($N_D = 5 \times 10^{18}$ cm^{-3}) can indeed lead to TFETs with improved performance when compared to conventional TFETs with similar a drain doping concentration.

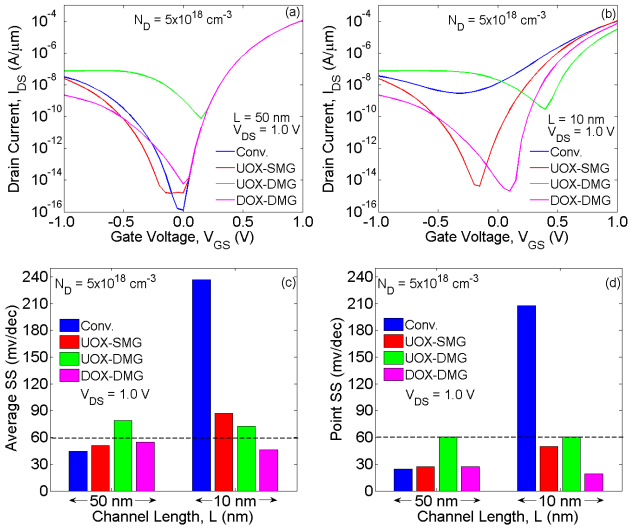

FIGURE 6. (a) Transfer characteristics for L = 50 nm, (b) transfer characteristics for L = 10 nm, (c) average SS and (d) point SS of the four different TFET structures with $N_D = 5 \times 10^{18}$ cm^{-3}.

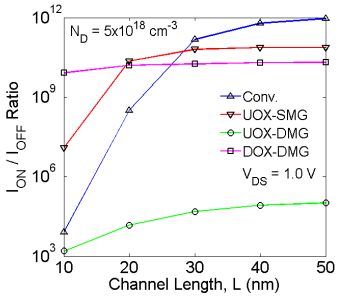

FIGURE 7. I_{ON}/I_{OFF} ratio versus channel length of the four different TFET structures where $I_{ON} = I_{DS}$ at $V_{GS} = 1.0$ V and $I_{OFF} = I_{DS}$ at $V_{GS} = 0.0$ V.

C. IMPACT OF THE GATE-ON-DRAIN OVERLAP ON TFETs FOR $N_D = 1 \times 10^{19}$ cm^{-3}

Fig. 8 shows the transfer characteristics, average SS and point SS of four different TFET structures for L = 50 nm and 10 nm with $N_D = 1 \times 10^{19}$ cm^{-3}. In Fig. 8, either for L = 50 nm or 10 nm, we observe that the conventional TFET exhibits undesirable ambipolar current. For L = 10 nm, the conventional TFET becomes unusable due to the extremely poor I_{ON}/I_{OFF} ratio and its subthreshold swing cannot be calculated due to the same reason. For the four TFET structures, the average and point SS, are shown in Figs. 8 (c) and (d), respectively and their I_{ON}/I_{OFF} ratios are shown in Fig. 9. These results show that as compared to the conventional TFET, the DOX-DMG TFET exhibits an OFF-state current $\approx 10^{-14}$ A/μm and an I_{ON}/I_{OFF} ratio $\approx 10^{10}$ when $N_D = 1 \times 10^{19}$ cm^{-3}.

From the above discussions, it is clear that the UOX-DMG TFET with $N_D = 1 \times 10^{18}$ cm^{-3} and DOX-DMG TFET with $N_D = 1 \times 10^{18}$ cm^{-3} to 5×10^{18} cm^{-3} are promising candidates for realizing TFETs with a low OFF-state current, an average SS less than 60 mV/dec and a high I_{ON}/I_{OFF} ratio. To understand the reason for the sub-60 mV/dec subthreshold swing and a low OFF-state current in the UOX-DMG TFET

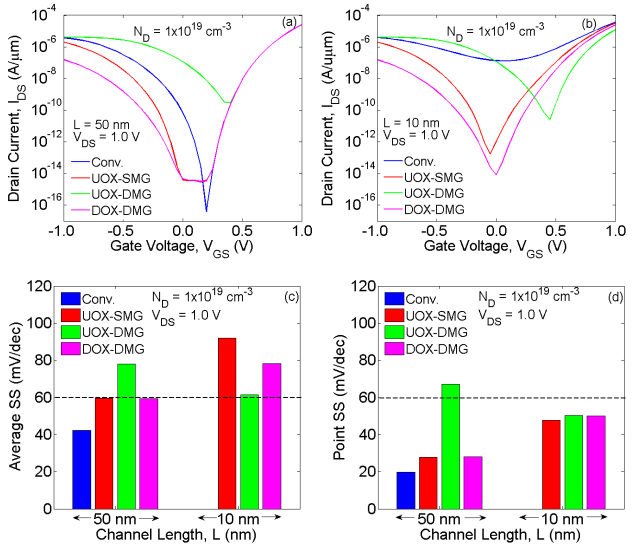

FIGURE 8. (a) Transfer characteristics for L = 50 nm, (b) transfer characteristics for L = 10 nm, (c) average SS and (d) point SS of the four different TFET structures with $N_D = 1 \times 10^{19}$ cm^{-3}.

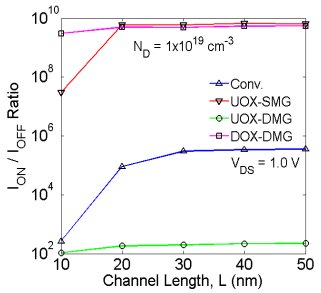

FIGURE 9. I_{ON}/I_{OFF} ratio versus channel length of the four different TFET structures where $I_{ON} = I_{DS}$ at $V_{GS} = 1.0$ V and $I_{OFF} = I_{DS}$ at $V_{GS} = 0.0$ V.

and DOX-DMG TFET with a drain doping concentration 1×10^{18} cm$^{-3} < N_D < 5 \times 10^{18}$ cm^{-3}, we have investigated the impact of channel length on the threshold voltage in the following section.

D. REVERSE SHORT CHANNEL EFFECTS

As shown in Fig. 10, the threshold voltage (V_t), i.e. the V_{GS} when $I_{DS} = 1 \times 10^{-7}$ A/μm, of the four different TFET structures is extracted at different channel lengths from 50 nm to 10 nm for three drain doping concentrations $N_D = 1 \times 10^{18}$ cm^{-3}, 5×10^{18} cm^{-3} and 1×10^{19} cm^{-3}. From Figs. 10 (a) – (c), we observe that the V_t of the conventional TFET decreases, as the channel length is scaled down, exhibiting the conventional V_t roll-off. The V_t for the conventional TFET with $N_D = 1 \times 10^{19}$ cm^{-3} and L = 10 nm is not shown in Fig. 10 (c), since it cannot be calculated due to the extremely poor I_{ON}/I_{OFF} ratio as seen in Fig. 9. However, as shown in Fig. 10 (a) with $N_D = 1 \times 10^{18}$ cm^{-3} and (b) with $N_D = 5 \times 10^{18}$ cm^{-3}, the UOX-DMG TFET and DOX-DMG TFET exhibit a threshold voltage roll-up when L is reduced from 50 nm to 10 nm. This is a clear indication of the presence of the reverse short channel effect as the channel length is scaled down. In contrast, as shown in

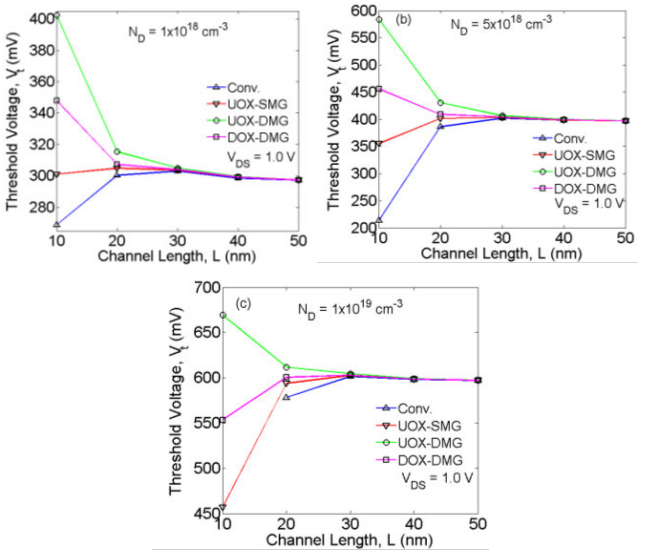

FIGURE 10. Comparison of the threshold voltage of the four different TFET structures at different channel lengths with drain doping concentrations (a) $N_D = 1 \times 10^{18}$ cm^{-3}, (b) $N_D = 5 \times 10^{18}$ cm^{-3} and (c) $N_D = 1 \times 10^{19}$ cm^{-3}.

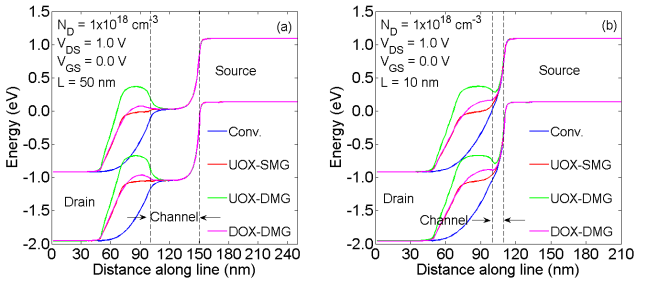

FIGURE 11. Energy-band profiles at 1 nm below the Si – SiO_2 interface of the four different TFET structures at $V_{GS} = 0.0$ V for (a) L = 50 nm and (b) L = 10 nm.

Fig. 10 (c) for $N_D = 1 \times 10^{19}$ cm^{-3}, the V_t of the DOX-DMG TFET decreases as the channel length is scaled from 50 nm to 10 nm exhibiting the conventional V_t roll-off. This V_t roll-off is the possible reason for the non-ideal subthreshold swing in DOX-DMG TFET with $N_D = 1 \times 10^{19}$ cm^{-3}. The reason for the reverse short channel effect in UOX-DMG TFET and DOX-DMG TFET can be understood by studying the energy band profiles for L = 50 nm and 10 nm at $V_{GS} = 0.0$ V, as discussed below.

E. DRAIN INDUCED BARRIER WIDENING (DIBW)

Figs. 11 (a) and (b) show the energy-band profiles of the four different TFET structures for L = 50 nm and 10 nm, respectively, with $N_D = 1 \times 10^{18}$ cm^{-3} at $V_{GS} = 0.0$ V. It can be observed from Fig. 11 (a) that in the presence of gate-on-drain overlap, there is an increased barrier height in the energy bands under the gate-on-drain overlap when compared to the conventional TFET. Since $\Phi_{OL} > \Phi_G$ in UOX-DMG TFET, the energy barrier height under the gate-on-drain overlap is higher when compared to the UOX- SMG TFET in which $\Phi_{OL} = \Phi_G$. However, in the case of DOX-DMG TFET, even

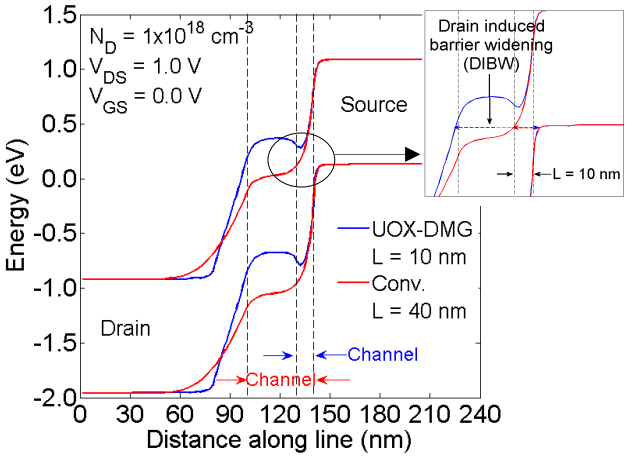

FIGURE 12. Energy-band profiles at 1 nm below the Si – SiO_2 interface of the UOX-DMG TFET with L = 10 nm and conventional TFET with L = 40 nm at V_{GS} = 0.0 V.

though $\Phi_{OL} > \Phi_G$, the energy barrier height under the gate-on-drain overlap decreases, since the oxide thickness under the gate-on-drain overlap ($t_{OX,OL}$) in DOX-DMG TFET is larger than its gate oxide thickness (t_{OX}). This reduction in barrier height is due to the reduced capacitive coupling when compared to the UOX-DMG TFET. It can be observed from Fig. 11 (b) that as the channel length is scaled from 50 nm to 10 nm, the distance between the source-channel junction and the induced barrier height due to the gate-on-drain overlap has also reduced. This proximity modulates the energy profile in the channel region resulting in the drain induced barrier widening (DIBW), at the source-channel junction, a phenomenon observed for the first time in TFETs. DIBW results in an increase in the tunnel width at the source-channel junction in the UOX-SMG TFET, UOX-DMG TFET and DOX-DMG TFET as compared to the conventional TFET as shown in Fig. 11 (b). The presence of drain induced barrier widening at the source-channel junction implies that a higher V_{GS} must be applied in UOX-DMG TFET and DOX-DMG TFET to achieve an I_{DS} equal to that of the 50 nm TFET. We can, therefore, conclude that in order to observe the reverse short channel effect in a TFET i.e. threshold voltage roll-up, the TFET must have a gate-on-drain overlap (with $\Phi_{OL} > \Phi_G$) and a channel length, $L \leq 20$ nm.

Fig. 12 shows the energy-band profiles of the UOX-DMG and conventional TFETs for L = 10 nm and 40 nm, respectively, with $N_D = 1 \times 10^{18}$ cm^{-3} at $V_{GS} = 0.0$ V. It is apparent that the tunnel width at the source-channel junction of the UOX-DMG TFET is larger when compared to the conventional TFET, clearly indicating the presence of drain induced barrier widening (DIBW) induced by the gate-on-drain overlap. As reported in this work, DIBW is responsible for the steep subthreshold swing and reduced OFF-state current in TFETs with gate-on-drain overlap.

V. CONCLUSION

With the help of calibrated 2-D simulations, we have successfully demonstrated in this paper how the performance of a TFET can be improved by using a new phenomenon known as the drain induced barrier widening (DIBW) at the source-channel junction. We also demonstrate that due to an increase in the tunneling width at the source-channel junction caused by DIBW, the TFETs exhibit reverse short channel effects. By exploiting DIBW, we have shown how TFETs can maintain a sub-60 mV/dec average subthreshold swing (≈35 mV/dec), a low OFF-state current ($\approx 10^{-16}$A/μm) and an I_{ON}/I_{OFF} ratio $\approx 10^{11}$ with drain doping concentrations as high as $N_D = 5 \times 10^{18}$ cm^{-3}. Our results may serve as a strong incentive for the experimental realization of TFETs with improved performance.

REFERENCES

[1] S. Saurabh and M. J. Kumar, *Fundamentals of Tunnel Field-Effect Transistors*. Boca Raton, FL, USA: CRC Press, Oct. 2016.

[2] R. Vishnoi and M. J. Kumar, "An accurate compact analytical model for the drain current of a TFET from subthreshold to strong inversion," *IEEE Trans. Electron Devices*, vol. 62, no. 2, pp. 478–484, Feb. 2015, doi: 10.1109/TED.2014.2381560.

[3] W. C.-Y. Ma and S.-M. Luo, "Impacts of stress voltage and channel length on hot-carrier characteristics of tunnel field-effect thin-film transistor," *IEEE Trans. Electron Devices*, vol. 67, no. 11, pp. 5243–5246, Nov. 2020, doi: 10.1109/TED.2020.3025741.

[4] K. Boucart and A. M. Ionescu, "Double-gate tunnel FET with high-*k* gate dielectric," *IEEE Trans. Electron Devices*, vol. 54, no. 7, pp. 1725–1733, Jul. 2007, doi: 10.1109/TED.2007.899389.

[5] M. J. Kumar and S. Janardhanan, "Doping-less tunnel field effect transistor: Design and investigation," *IEEE Trans. Electron Devices*, vol. 60, no. 10, pp. 3285–3290, Oct. 2013, doi: 10.1109/TED.2013.2276888.

[6] K.-M. Liu and C.-P. Cheng, "Investigation on the effects of gate-source overlap/underlap and source doping gradient of n-type Si cylindrical gate-all-around tunnel field-effect transistors," *IEEE Trans. Nanotechnol.*, vol. 19, pp. 382–389, 2020, doi: 10.1109/TNANO.2020.2991787.

[7] C.-H. Shih and N. D. Chien, "Sub-10-nm tunnel field-effect transistor with graded Si/Ge heterojunction," *IEEE Electron Device Lett.*, vol. 32, no. 11, pp. 1498–1500, Nov. 2011, doi: 10.1109/LED.2011.2164512.

[8] Y. J. Yoon, J. H. Seo, S. Cho, H.-I. Kwon, J.-H. Lee, and I. M. Kang, "Effects of dual-spacer dielectrics on low-power and high-speed performance of sub-10 nm tunneling field-effect transistors," *Jpn. J. Appl. Phys.*, vol. 55, no. 6S1, 2016, Art. no. 06GG02.

[9] J. Wu and Y. Taur, "Reduction of TFET OFF-current and subthreshold swing by lightly doped drain," *IEEE Trans. Electron Devices*, vol. 63, no. 8, pp. 3342–3345, Aug. 2016, doi: 10.1109/TED.2016.2577589.

[10] J. Z. Huang, P. Long, M. Povolotskyi, G. Klimeck, and M. J. W. Rodwell, "Scalable GaSb/InAs tunnel FETs with nonuniform body thickness," *IEEE Trans. Electron Devices*, vol. 64, no. 1, pp. 96–101, Jan. 2017, doi: 10.1109/TED.2016.2624744.

[11] D. B. Abdi and M. J. Kumar, "Controlling ambipolar current in tunneling FETs using overlapping gate-on-drain," *IEEE J. Electron Devices Soc.*, vol. 2, no. 6, pp. 187–190, Nov. 2014, doi: 10.1109/JEDS.2014.2327626.

[12] Y. Yang, X. Tong, L. Yang, P. Guo, L. Fan, and Y. Yeo, "Tunneling field-effect transistor: Capacitance components and modelling," *IEEE Electron Device Lett.*, vol. 31, no. 7, pp. 753–754, Jul. 2010.

[13] X. Zhou and W. Long, "A novel hetero-material gate (HMG) MOSFET for deep-submicron ULSI technology," *IEEE Trans. Electron Devices*, vol. 45, no. 12, pp. 2546–2548, Dec. 1998.

[14] W. Long, H. Ou, J.-M. Kuo, and K. K. Chin, "Dual-material gate (DMG) field effect transistor," *IEEE Trans. Electron Devices*, vol. 46, no. 5, pp. 865–870, May 1999.

[15] S. Song, Z. Zhang, M. Hussain, C. Huffman, J. Barnett, S. Bae, H. Li, P. Majhi, C. Park, B. Ju, H. K. Park, C. Y. Kang, R. Choi, P. Zeitzoff, H. H. Tseng, B. H. Lee, and R. Jammy, "Highly manufacturable 45 nm LSTP CMOSFETs using novel dual high-k and dual metal gate CMOS integration," in *VLSI Symp. Tech. Dig.*, 2006, pp. 13–14.

[16] I. Polishchuk, P. Ranade, T.-J. King, and C. Hu, "Dual work function metal gate CMOS technology using metal interdiffusion," *IEEE Electron Device Lett.*, vol. 22, no. 9, pp. 444–446, Sep. 2001.

[17] C. Ren, H. Yu, J. Kang, X. Wang, H. Ma, Y. Yeo, D. Chan, M. Li, and D. Kwong, "A dual-metal gate integration process for CMOS with sub1-nm EOT HfO_2 by using HfN replacement gate," *IEEE Electron Device Lett.*, vol. 25, no. 8, pp. 580–582, Aug. 2004.
[18] Y.-C. Yeo, Q. Lu, P. Ranade, H. Takeuchi, K. J. Yang, I. Polishchuk, T.-J. King, C. Hu, S. C. Song, H. F. Luan, and D. L. Kwong, "Dual-metal gate CMOS technology with ultrathin silicon nitride gate dielectric," *IEEE Electron Device Lett.*, vol. 22, no. 5, pp. 227–229, May 2001.
[19] D.-G. Lin, S. L. Tu, Y.-C. See, and P. Tam, "A novel LDMOS structure with a step gate oxide," in *IEDM Tech. Dig.*, 1995, pp. 963–966, doi: 10.1109/IEDM.1995.499376.
[20] X. Liao, K. K. P. Tsui, H. Liu, K. J. Chen, and J. K. O. Sin, "A step-gate-oxide SOI MOSFET for RF power amplifiers in short- and medium-range wireless applications," in *Proc. Meeting Silicon Monolithic Integr. Circuits RF Syst.*, 2003, pp. 33–36, doi: 10.1109/SMIC.2003.1196662.
[21] H. Xing, Y. Dora, A. Chini, S. Heikman, S. Keller, and U. K. Mishra, "High breakdown voltage AlGaN-GaN HEMTs achieved by multiple field plates," *IEEE Electron Device Lett.*, vol. 25, no. 4, pp. 161–163, Apr. 2004, doi: 10.1109/LED.2004.824845.
[22] *ATLAS Device Simulation Software*, Silvaco, Santa Clara, CA, USA, 2016.
[23] S. Garg and S. Saurabh, "Exploiting within-channel tunneling in a nanoscale tunnel field-effect transistor," *IEEE Open J. Nanotechnol.*, vol. 1, pp. 100–108, 2020, doi: 10.1109/OJNANO.2020.3031633.
[24] S. Garg and S. Saurabh, "Improving the scalability of SOI-based tunnel FETs using ground plane in buried oxide," *IEEE J. Electron Devices SoC.*, vol. 7, no. 1, pp. 435–443, Apr. 2019, doi: 10.1109/JEDS.2019.2907314.
[25] G. Musalgaonkar, S. Sahay, R. S. Saxena, and M. J. Kumar, "A line tunneling field-effect transistor based on misaligned Core–Shell gate architecture in emerging nanotube FETs," *IEEE Trans. Electron Devices*, vol. 66, no. 6, pp. 2809–2816, Jun. 2019.

MAMIDALA KARTHIK RAM was born in New Delhi, India. He received the bachelor's degree in electronics and communication engineering from NIIT University, Neemrana, India. He is currently pursuing the master's degree in nanoscience with Lund University, Lund, Sweden. He carried out research in the area of nanoscale MOSFETs as an Intern at IIIT Delhi, India. His research interests include nanoelectronic devices, low-power transistors, and TCAD.

NEHA TIWARI received the M.Tech. degree in digital communications and the Ph.D. degree in nanoelectronics from Barkatullah University, Bhopal. Before joining NIIT University (NU), she was an Assistant Professor with the University Institute of Technology, Barkatullah University, for a period of ten years. She is currently an Assistant Professor with the Electronics and Communication Engineering Department, NU, where she teaches optic and satellite communications.

DAWIT BURUSIE ABDI received the B.Sc. degree in electrical engineering from Jimma University, Ethiopia, in 2009, the M.Tech. degree in microelectronics from the Addis Ababa Institute of Technology, Ethiopia, in 2011, and the Ph.D. degree from the Department of Electrical Engineering, Indian Institute of Technology Delhi, New Delhi, India. He is currently a Postdoctoral Researcher at IMEC, Leuven, Flemish Region, Belgium. His current research interests include design, simulation, and modeling of nanoscale semiconductor devices.

SNEH SAURABH (Senior Member, IEEE) received the B.Tech. degree in electrical engineering from IIT Kharagpur, Kharagpur, India, in 2000, and the Ph.D. degree from IIT Delhi, New Delhi, in 2012. He is currently an Associate Professor with the Department of Electronics and Communication Engineering, Indraprastha Institute of Information Technology (IIIT) Delhi, New Delhi. Before joining IIIT Delhi, in June 2016, he worked in the semiconductor industry for around 16 years. His current research interests include nanoelectronics, exploratory electronic devices, energy efficient systems, and CAD for VLSI. He is also an Editor of the *IETE Technical Review* and an Associate Editor of IEEE.